

Critical Hydrogen Coverage Effect on the Hydrogenation of Ethylene Catalyzed by δ -MoC (001): An *Ab Initio* Thermodynamic and Kinetic Study

Carlos Jimenez-Orozco,^{†*} Elizabeth Florez,[†] Francesc Viñes,^{‡*} José A. Rodríguez,[§] Francesc Illas[‡]

[†]*Universidad de Medellín, Facultad de Ciencias Básicas, Grupo de Materiales con Impacto, Mat&mpac, Carrera 87 No 30-65, Medellín, Colombia*

[‡]*Universitat de Barcelona, Departament de Ciència de Materials i Química Física & Institut de Química Teòrica i Computacional (IQTCUB), c/ Martí i Franquès 1-11, 08028 Barcelona, Spain.*

[§]*Brookhaven National Laboratory, Chemistry Department, Upton, New York 11973, United States of America*

ABSTRACT

The molecular mechanism of ethylene (C₂H₄) hydrogenation on a δ -MoC (001) surface has been studied by periodic density functional theory methods. Activation energy barriers and elementary reaction rates have been calculated as a function of the hydrogen surface coverage, θ_{H} , with relevant properties derived from *ab initio* thermodynamics and kinetic rate estimates. The hydrogen coverage has a very strong effect on the adsorption energy and the second hydrogenation step of ethylene. A relatively low energy barrier favors the dissociation of H₂ on δ -MoC (001) leading to medium H coverages (> 0.4 of a monolayer) where the energy barrier for the full hydrogenation of ethylene is already below the corresponding barriers seen on Pt and Pd (111). At a high H coverage of ~0.85 of a monolayer, the C₂H₄ adsorbs at 1 atm and 300 K over a system having as-formed CH₃ moiety species, which critically favors the C₂H₄ second hydrogenation, typically a rate limiting step, by reducing its activation energy to a negligible value of 0.08 eV, significantly lower than the equivalent values of ~0.5 eV reported for Pt and Pd (111) catalyst surfaces. The ethane desorption rate is larger than the surface intermediate elementary reaction rates, pointing for its desorption upon formation, closing the catalytic cycle. The present results put δ -MoC under the spotlight as an economic and improved replacement catalyst to Pt and Pd, with significant improvements in enthalpy and activation energy barriers. Here, we provide a detailed study for the C₂H₄ hydrogenation reaction mechanism over a carbide showing characteristics or features not seen on metal catalysts. These can be exploited when dealing with technical or industrial applications.

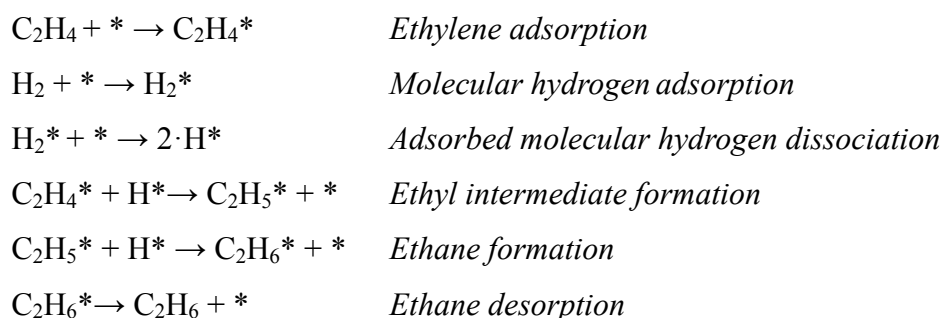
*Corresponding authors: Carlos Jimenez-Orozco: cjimenez@udem.edu.co, Francesc Viñes: francesc.vines@ub.edu

Keywords: Hydrogenation · Ethylene · δ -MoC · Density Functional Calculations · Coverage

INTRODUCTION

Hydrogenation reactions are key processes in the chemical industry. Several commodities and chemicals are produced *via* the hydrogenation of unsaturated C-C double bonds in olefins. Their effective hydroconversion normally requires heterogeneous catalysts, where the most used ones belong to the Pt-group metals —*a.k.a.* platinoids; Ru, Rh, Pd, Os, Ir, and Pt.¹ However, the Pt scarcity in the Earth crust leads to a high market price, thus limiting such Pt-based catalysts applications at large scales, which are necessary for the growing demand of such relevant chemical products. Additionally, the use of Pt-group metals in the petrochemical industry is of primary importance in the production of clean fuels, currently limited by the presence of heteroatoms like sulfur and nitrogen in crude oil, poisoning the Pt-based-group metals.² Therefore, alternative materials are necessary to overcome these issues, and over the years transition metal carbides have been proposed as low-cost promising materials.²⁻⁵ Among these compounds, molybdenum carbide has shown a very good potential as a technical catalyst for hydrogenation reactions,^{2,6-10} as shown both by experimental and theoretical studies. The cubic phase of molybdenum carbide, *i.e.* δ -MoC, has shown substantial catalytic activity for CO₂ hydrogenation,^{6,11} the low temperature water gas-shift reaction,^{10,12} and hydrogen dissociation.^{13,14} Here we investigate the hydrogenation process on a δ -MoC (001) non-polar surface, which contains stoichiometric quantities of both C and Mo atoms, allowing the reactivity study on both types of centers.^{15,16} The (001) surface choice is backed up being the δ -MoC most stable one, featured in its vast majority on δ -MoC crystallites according to the Wulff construction of nanoparticle shapes, minimizing the materials surface tension.¹⁶

Ethylene or ethene (C₂H₄) is the simplest olefin molecule, and a useful probe chemical frequently employed to understand the hydrogenation of unsaturated C=C double bonds. Particularly, this process has been widely documented on Pt and Pd (111) surfaces, the most stable ones on such metals, and, therefore, the most exposed in supported metallic Pt and Pd nanoparticles when used as catalysts. It is well established that C₂H₄ hydrogenation on Pt-group metal surfaces follows a Horiuti-Polanyi mechanism —a Langmuir-Hinshelwood-like type of mechanism where both reactants are adsorbed on the catalyst.¹⁷ Briefly, the reaction mechanism consists of the following six steps:



On both Pt^{18–20} and Pd^{21–23} (111) surfaces the ethane (C₂H₆) production rate is found to increase with the hydrogen (H₂) partial pressure. In other words, C₂H₄ hydrogenation is favored at a high hydrogen surface coverage, θ_{H} . Even though ethylene adsorption has been studied on some transition metal carbides (TMCs),²⁴ and its hydrogenation partially explored in some TaC²⁵ and WC²⁶ based catalysts, there is still a lack of knowledge regarding the details of the C₂H₄ hydrogenation reaction mechanism on such materials. Here, we specifically address this reaction on the δ -MoC (001) catalyst, given its suitable interaction with ethylene and H₂ as reported in previous works.^{13,27}

In the context of the reaction mechanism, the interaction of ethylidyne (CCH₃) with the surface has to be regarded since, on Pt-based catalysts, it is known that it can be a poisoning species.²⁸ Nevertheless, on TMC surfaces its possible hydrogenation towards ethyl or ethane has been suggested, ruling out its poison activity.²⁹ At variance to the well-studied Pt and Pd (111) metal surfaces where, once formed, ethylidyne becomes strongly bonded and hardly modified, thus becoming a blocker of active sites, on δ -MoC (001) and some other TMCs there is a thermodynamic driving force to transform this adsorbed species into other desirable hydrocarbons; thus preventing a catalyst deactivation mechanism.²⁹ The different chemistry towards ethylidyne suggests that δ -MoC (001) can be a very good candidate to replace Pt-group metals as a catalyst for olefin hydrogenation reactions, pointing to the need for more in-depth studies. In this aspect, it is important to understand the role of the hydrogen coverage in the hydrogenation of adsorbed ethylene, as one has to regard that hydrogenation reactions are usually carried out in hydrogen-rich environments.^{18,19,30} This also should be valid on the δ -MoC (001) surface, where a relatively small energy barrier of 0.39 eV for H₂ dissociation has been gained, from a previously physisorbed molecular adsorption state, fostering an easy H₂ uptake, dissociation, and high-coverage of adatomic H upon.¹⁴ Indeed, the structurally similar TiC (001) surface shows a diversity of H species, adsorbed on top of C or Ti atoms, even elongated H₂ *Kubas* modes, that are predicted to remain at temperatures in the 300-400 K interval, a range relevant for hydrogenation processes,³¹ plus a systematic analysis of H₂ adsorption and dissociation on molybdenum carbide surfaces reveals that CH₃-like species can be formed at high hydrogen surface coverages, as observed on C-terminated β -Mo₂C (001) surface.¹³ However, such moieties were not inspected on δ -MoC (001) surfaces, nor their possible influence, *e.g.* in the chemical activity towards ethylene hydrogenation.

The goal of the present work is to get unbiased insights on C₂H₄ hydrogenation as catalyzed by δ -MoC (001). In particular, the aim is set at evaluating the ethylene binding energy as a function of adsorbed hydrogen coverage, θ_{H} , and the influence of the employed working conditions. To this end, situations with θ_{H} in the 0.13 to 0.88 monolayers (ML) range have been investigated, regarding a 1 ML when all δ -MoC surface atoms are occupied by an adsorbate. Besides, the effect of

temperature and H_2/C_2H_4 pressure on the interaction of ethylene with the carbide surface at given θ_H coverages has been studied by means of the so-called *ab initio* thermodynamics (AIT) formalism, as described by Reuter and Scheffler.^{32,33} Finally, the kinetics of C_2H_4 hydrogenation through the Horiuti-Polanyi-like mechanism has been explored by determining the relevant reaction step energy barriers, which are compared to the ones obtained on Pt and Pd (111) surfaces. Finally, transition state theory (TST) has been used to investigate the ethane desorption rate and the elementary reaction rates dependence with temperature. The reported information provides a complete thermodynamic and kinetic panorama of C_2H_4 hydrogenation on δ -MoC (001) through a Horiuti-Polanyi-like reaction mechanism, identifying as well similarities and differences with respect to the commonly used metal catalysts.

MODELS AND METHODS

The δ -MoC (001) surface has been represented by a periodic supercell slab model built from the previously optimized bulk structure, with a vacuum region between interleaved slabs of 15 Å. The slab model contains six atomic layers which deliver converged calculated ethylene adsorption energies with respect the slab thickness, as earlier also verified in the ethylene interaction on the similar system of tungsten carbide.²⁴ The positions of the four bottommost atomic layers were fixed at bulk values to provide an appropriate environment to the two outermost layers, whose structure was fully relaxed. The employed supercell is a $(2\sqrt{2}\times 2\sqrt{2})R45^\circ$ —76.37 Å² of area— containing a total of 96 atoms, 48 C and 48 Mo, with 8 C and 8 Mo atoms per slab atomic layer. Similar models have been used in past studies on the adsorption^{34,35} and reactivity of chemicals on similar TMCs.³⁶ The supercell size on ethylene adsorption was evaluated *vs.* an equivalent $(3\sqrt{2}\times 3\sqrt{2})R45^\circ$ model, featuring negligible changes with supercell size and coverage; see detailed discussion and Figure S1 of the Supporting Information (SI).

To investigate the effect of pre-adsorbed hydrogen on the overall process, several θ_H values have been considered implying a different number of H adatoms (H^*) in the supercell surface model, *i.e.* 0.13 (2 H^*), 0.25 (4 H^*), 0.38 (6 H^*), 0.50 (8 H^*), 0.63 (10 H^*), 0.75 (12 H^*), and 0.88 ML (14 H^*), well within the limits observed for less H-affine TiC(001) surface.³¹ Notice that when hydrogenating C_2H_4 , the effective θ_H decays 2 H^* —0.13 ML, or 0.067 ML per hydrogenation step— although given the little impact on θ_H on the reaction energetics, we will refer in the following to the initial considered θ_H , this is, before C_2H_4 first hydrogenation step. For θ_H coverage values ranging from 0.13 to 0.50 ML H^* occupies surface C sites, as predicted in previous works.^{13,14} For larger H^* coverages, H^* starts to populate atop of surface Mo atoms.¹³ The stages for all the evaluated surface coverages are shown in Figure S2 of the SI. The C_2H_4 adsorption energy was evaluated for each θ_H with the structure of the adsorbed molecule fully relaxed. For the

sake of clarity, note that the C₂H₄ bonding mode on the clean δ -MoC (001) surface has been earlier exhaustively studied, and reported to be atop of a surface Mo atom — π -M mode—²⁷ in a Type-I group of C-C bond elongation;²⁴ and such ethylene has been maintained on such during the several studied pre-adsorbed H* atoms situations. Notice also that θ_H values larger than 0.88 ML have not been considered, since ethylene adsorption would require, obviously, at least a free surface Mo site. For $\theta_H = 0.88$ ML, the total net coverage of surface sites —this is, including H* and C₂H₄*— is 0.94 ML, with the remaining 0.06 ML free site being a Mo surface atom. Therefore, the model with $\theta_H = 0.88$ ML contains an even number of H* atoms, all coming from H₂ molecules dissociated at the surface. For practical purposes, the thermodynamics and kinetics aspects were further evaluated on three representative limiting cases of low, medium, and high θ_H of 0.13, 0.50, and 0.88 ML, respectively.

The total energy of the above-mentioned supercell models has been calculated using a periodic density functional theory (DFT) approach, and the corresponding equilibrium structures obtained from standard total energy minimization procedures. The DFT calculations were carried out using the Vienna *ab initio* simulation package (VASP) code,³⁷ using the Perdew-Burke-Ernzerhof (PBE) functional,³⁸ especially well-suited in the description of Mo-based carbides.³⁹ For all the evaluated systems, the dispersive forces were added through the D3 approach, *i.e.* PBE-D3.⁴⁰ The valence electron density was expanded in a plane-wave basis set with an associate kinetic energy not surpassing a 400 eV cutoff value. The description of the effect of the inner electrons in the valence region is described by the projected augmented wave (PAW) method⁴¹ as implemented by Kresse and Joubert.⁴² For the numerical integration in the Brillouin zone, according to the Monkhorst–Pack scheme,⁴³ a Γ -centered \mathbf{k} -points mesh of $3 \times 3 \times 1$ was used for the necessary numerical integrations involving the periodic supercell representation of δ -MoC(001). The convergence criteria were changes in total energies lower than 10^{-6} eV and variations in interatomic forces lower than $0.01 \text{ eV} \cdot \text{\AA}^{-1}$. Moreover, a dipole correction was used to avoid dipole coupling between repeated slabs.

The ethylene adsorption energy, E_{ads} , was calculated as

$$E_{\text{ads}} = E_{\text{C}_2\text{H}_4/\text{MoCH}_n} - E_{\text{MoCH}_n} - E_{\text{C}_2\text{H}_4} \quad (1),$$

including the zero point energy (ZPE) in all terms, see Eq. S1 in the SI. Here the $E_{\text{C}_2\text{H}_4/\text{MoCH}_n}$ refers to the energy of the system with the adsorbed C₂H₄ on the δ -MoC (001) surface containing n H* adatoms, $E_{\text{C}_2\text{H}_4}$ stands for the isolated molecule energy, and E_{MoCH_n} the energy of the δ -MoC (001) surface containing n H* atoms without C₂H₄ molecule. The vibrational frequencies needed for, e.g. the ZPE term, have been computed within the harmonic approximation considering the adsorbates vibrational frequencies only, gained through the diagonalization of the Hessian matrix with finite

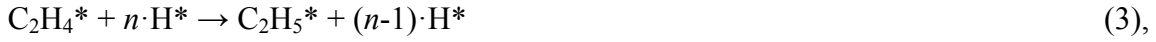
differences elements computed through analytical gradients with displacements of the coordinates of the involved atoms of 0.01 Å.

The C₂H₄ Gibbs free energy of adsorption (ΔG_{ads}) for each considered situation case has been acquired within the AIT model as

$$\begin{aligned} \Delta G_{\text{ads}} = & E_{\text{ads}} - k_{\text{B}}T \left\{ \left[\ln(q_{\text{vib}}^{\text{ads}}) \right] - \left[\ln(q_{\text{vib}}^{\text{surf}}) \right] - \left[\ln \left(\left(\frac{2\pi m_{\text{C}_2\text{H}_4} k_{\text{B}}T}{h^2} \right)^{3/2} \frac{k_{\text{B}}T}{p_{\text{C}_2\text{H}_4}} \right) + \ln \left(\frac{\pi^{1/2}}{\sigma_{\text{r}}} \left(\frac{T^{3/2}}{(\Theta_{\text{x}}\Theta_{\text{y}}\Theta_{\text{z}})^{1/2}} \right) \right) \right] \right. \\ & \left. + \sum_{i=1}^{nvm} \ln \left(\left[\frac{1}{1 - \exp(-h\nu_i/k_{\text{B}}T)} \right] \right) \right\}_{\text{gas}} \end{aligned} \quad (2),$$

for additional details, we refer the reader to Equations S2-S4 of the SI.

For each situation with n H* atoms on the surface, the following elementary steps for a Horiuti-Polanyi mechanism, involving the C₂H₅* ethyl intermediate, were considered for the C₂H₄ hydrogenation.



For each elementary step, its transition state (TS) structures was located following a two-steps procedure. In the first one, a non-linear interpolation of a set of eight images provided by the atomistic simulation environment (ASE) package⁴⁴ was obtained. Next, the thus generated images were used to search for saddle points for the hydrogenation steps using the climbing-image nudged elastic band (CI-NEB) method.⁴⁵ The TS structure candidates were characterized *via* frequency analysis to ensure a single imaginary frequency in the desired reaction direction. In addition, the elementary reaction rate, r , and its temperature, T , dependence was estimated according to harmonic TST as applied to surface reactions,^{46,47}

$$r = \frac{k_{\text{B}}T}{h} \frac{q_{\text{vib}}^{\text{TS}}}{q_{\text{vib}}^{\text{IS}}} e^{-\frac{E_{\text{a}}}{k_{\text{B}}T}} \quad (6),$$

where IS refers to the initial state of the reaction step. Additional details and full explanation of the meaning of each term are provided in the SI. In a similar way, C₂H₆ desorption rate was obtained as

$$r_{\text{des}} = \frac{k_{\text{B}}T}{h} \nu_{\text{free}} e^{\frac{E_{\text{ads}}}{k_{\text{B}}T}} \quad (7),$$

with additional details on such terms provided in the SI.

RESULTS AND DISCUSSION

Ethylene Adsorption at Different H Surface Coverages. First, one has to recall the adsorption of C_2H_4 on δ -MoC(001), earlier found to be attached atop of a surface Mo atom π -M mode in a Type-I group of C-C bond elongation, with an adsorption energy on the previously found most stable site of -1.03 eV at PBE-D3 level.^{24,27} Regarding the effect of hydrogen coverage on the interaction between ethylene and δ -MoC(001) it is necessary to distinguish two regimes; for θ_H values of 0.13-0.75 ML (2-12 H^*), the most salient feature is a sharp decrease which is attributed to the Pauli repulsion between the H^* adatoms and ethylene, see Figure 1, and values and geometries found in Table S1 and Figure S3 of the SI. The effect is quite dramatic as the ethylene adsorption energy decreases 0.64-0.74 eV relative to the value corresponding to the clean, pristine surface. However, at high H^* coverage, *i.e.* for $\theta_H = 0.88$ ML involving 14 H^* in the supercells, ethylene adsorption *via* a π -mode spontaneously forces a rearrangement of the surface H^* adatoms resulting in CH_3 -like structures, see Figure S3 of the SI, not observed at lower coverages. These structures involve a surface C atom close the adsorbed ethylene molecule which is simultaneously attaching 3 H^* adatoms. The formation of this methyl-like surface structure induces a rather strong stabilization of the system, to the point that the adsorption energy of C_2H_4 becomes now -1.14 eV, even larger than the value for clean surface of -1.03 eV. This is quite a surprising result indicating that a rather high hydrogen partial pressure may be significantly beneficial. It is worth to mention that lateral interactions⁴⁸ between co-adsorbates are negligible, see discussion in SI.

To further analyze the thermodynamics involved in the C_2H_4 binding with a different extent of pre-adsorbed H^* atoms, three representative cases are considered next. Based on the results in Figure 1, we choose θ_H coverage values of 0.13, 0.50, and 0.88 ML. Figure 2 reports the optimized structure for each of these situations whereas Figures 3 and 4 report the estimated Gibbs free energy changes and analyze the effect of the ethylene partial pressure, $p_{C_2H_4}$, and temperature, T , on ethylene adsorption. The results for the full range of evaluated pressures and temperatures are reported in Table S2 of the SI.

Regarding the $p_{C_2H_4}$ effect in the C_2H_4 ΔG_{ads} , Figure 3 shows that, for the clean and high hydrogen coverage situations, there is quite a broad range of values where ethylene adsorption is predicted to be thermodynamically favored at 300 K, encompassing vacuum conditions of 10^{-10} atm and high pressures of 100 atm. However, for the low and intermediate H^* situations (θ_H of 0.13 and 0.50 ML, respectively) adsorption at 300 K is not favored, although this may perhaps be reversed at cryogenic, non-practical temperatures. Interestingly, the fact that at the high coverage of 0.88 ML C_2H_4 adsorption is feasible and with the adsorbed molecule surrounded by H^* , strongly suggests that hydrogenation is likely to proceed even at moderate $p_{C_2H_4}$ values of 10^{-7} onwards. On the other side of the coin, Figure 4 reports the calculated adsorption Gibbs free energy for a fixed $p_{C_2H_4}$ of 1 atm as a function of temperature. Figure 4 shows that C_2H_4 adsorption is thermodynamically

avored up to *circa* 200 K regardless of the H* coverage. However, above 200 K C₂H₄ adsorption becomes thermodynamically non-favored for θ_H of 0.13 and 0.50 ML but remains favored up to 400 K for the case of $\theta_H = 0.88$ ML and up to 700 K for the clean surface. Note that any increase of $p_{C_2H_4}$ implies that adsorption is thermodynamically favored only at lower temperatures, still accessible for $\theta_H = 0.88$ ML, but impossible for lower H* coverages. Once thermodynamic C₂H₄ adsorptive equilibrium states have been defined, kinetic aspects of the C₂H₄ hydrogenation and the ethane product desorption are addressed in the next point.

Influence of θ_H on the C₂H₄ Hydrogenation and C₂H₆ Desorption Kinetics. In spite of the apparent simplicity of the mechanism of C₂H₄ hydrogenation, summarized in Eqs. 3-5, the exploration of the potential energy surface for the case with $\theta_H = 0.13$ ML reveals that a larger number of elementary steps are involved in each elementary step, as shown in Figures S4 and S5 of the SI. Four of these steps correspond to H* migration steps so as to reach a proper attack angle from which hydrogenate the C₂H₄* or C₂H₅* moieties, plus there is also an activation step of the C₂H₄* moiety, so as to reach an adsorption C₂H₄* conformational isomer, which fosters its first hydrogenation. From the appropriate surface configurations for C₂H₄* and H* the reaction to produce C₂H₅* and a free surface site proceeds through a transition state, TS¹, involving an activation barrier of 0.47 eV, see Figure 5. However, the second hydrogenation; C₂H₅* + H* → C₂H₆* + *, proceeding through TS²—see Figure 5 and Figure S5 of the SI— involves a very large barrier of 1.71 eV at $\theta_H = 0.13$ ML. It is worth to mention that H* migrations and C₂H₄* isomerization steps are only seen for $\theta_H = 0.13$ ML, as increasing the θ_H to 0.50 and 0.88 ML one avoids these additional steps. At a θ_H of 0.50 ML both barriers are decreased to 0.40 and 0.36 eV, respectively, see Figure 5 and Figure S5 of the SI, indicating that a larger θ_H may have a beneficial effect, even if this would have a concomitant decrease on the ethylene adsorption energy.

However, as above-commented, when θ_H reaches 0.88 ML the ethylene adsorption becomes even more favorable than on the clean surface. In addition, calculations show that at this high θ_H , even though the energy barrier for the first hydrogenation through TS¹ is kept at 0.59 eV, the second energy barrier involving TS² dramatically decreases to solely 0.08 eV, see Figure 5 and Figure S7. Interestingly, the energy barriers for the first hydrogenation at θ_H of 0.13, 0.50, and 0.88 ML exhibit little variations, and are close to that reported for Pt^{49,50} and Pd^{49,51} (111) surfaces, of 0.49 and of 0.55 eV, respectively. To the best of our knowledge, for these two metal surface catalysts the effect of surface coverage has been limited to ethylene,⁴⁷ and there is no information regarding the effect of the hydrogen coverage on the ethylene hydrogenation energy profile, even though there are a couple of reports for Pt (111) surface involving high coverages, with θ_H from 0.25 to above 1 ML,^{52,53} yet without considering neither the ethylene adsorption nor its hydrogenation.

In the case of δ -MoC(001), we show here that the effect of hydrogen coverage on the C_2H_4 hydrogenation is quite large, provided it reaches a situation as high as $\theta_H = 0.88$ ML. Notice how the second hydrogenation energy barrier drops from 1.71 eV at 0.13 ML to merely 0.08 eV, much smaller than the reported values for Pt and Pd (111) surfaces of 0.55 and 0.52 eV, respectively.⁴⁹⁻⁵¹ Thus, θ_H plays a key role in the olefin hydrogenation *via* a Horiuti-Polanyi-like scheme on δ -MoC based catalysts, with high enough values resulting in quite low activation barriers. Note also that, for $\theta_H = 0.88$ ML, both hydrogenation elementary steps are exothermic while in the case of Pt and Pd (111) surfaces the first hydrogenation is thermoneutral, and the second one slightly exothermic. Therefore, on a δ -MoC based catalyst, the high hydrogen coverage does not only implies a change in the kinetics, due to the reduced activation energies, but also on the thermodynamics, improving the exothermic character of the adsorbed final product. Consequently, the θ_H coverage is the key parameter to improve both the thermodynamic and kinetic aspects of ethylene hydrogenation.

To understand the origin of the high-energy barrier for $\theta_H = 0.13$ ML of 1.71 eV and the collapse at 0.88 ML, with an energy barrier of 0.08 eV, we analyzed in detail the type of adsorbate-surface bonds in the system. At 0.13 ML there are several available surface C sites, so the $C_2H_5^*$ intermediate occupies one of these instead of a Mo site, see Figure S5, resulting in the formation of a strong $C_{\text{surface}}-C_{\text{ethyl}}$ covalent bond. Clearly, to hydrogenate $C_2H_5^*$ into $C_2H_6^*$ it is necessary to break this covalent bond, which involves a significant energetic toll. Increasing θ_H to 0.50 ML implies that all H^* species sit above C atoms, and this forces $C_2H_5^*$ to occupy a surface Mo atoms instead, see Figure S6, with a concomitant weaker Mo- $C_2H_5^*$ interaction. In fact, the energy barrier for this hydrogenation step decreases from 1.71 eV to 0.36 eV, a value already below the corresponding barriers for Pt and Pd (111) surfaces.

For the largest θ_H explored of 0.88 ML, the H^* atoms also occupy sites above Mo atoms,¹³ but some form surface CH_3 entities, as above-mentioned. At this coverage, the second hydrogenation was explored by using of one of the H^* atoms in such CH_3 entity or another available vicinal H^* atom. In the first case, the energy barrier to $C_2H_6^*$ becomes 0.60 eV, whereas on the second one leads to the lower barrier of 0.08 eV. Therefore, the CH_3 role is that of a matchmaker, allowing for another H^* to hydrogenate. For the $\theta_H = 0.88$ ML case, the system has been additionally characterized, particularly, concerning the temperature effect in the reaction rate, see Figure S8 of the SI. For a temperature 50 K, the rate-determining step is the first hydrogenation occurring through TS^1 , as expected. Hence, at a standard pressure, the reaction rates are similar in the range of 200–400 K. In particular, at 300 K, the reaction rates are sensibly large, of the order of 10^3 s⁻¹.

The results in the present work show that a high hydrogen surface coverage is advantageous in order to favor ethylene hydrogenation. This correlates, e.g. with other systems where an

improved performance is also favored at high hydrogen concentrations, as seen, *e.g.* in DFT-based results for benzene hydrogenation, found to be improved at a θ_{H} superior to 0.44 ML reducing the energy barriers,⁵⁴ although the benefit can be lateral, *i.e.* biasing the enantioselectivity of α -ketoesters hydrogenation.⁵⁵ Notice that olefins adsorption capability decreases θ_{H} , as the di- σ -MM mode shifts into π -M at high θ_{H} on Pt (111) surface. This aspect is key to understand the olefin hydrogenation mechanism on Pt-group-based metals,³⁰ where, experimentally, the performance is improved at high hydrogen concentrations,¹⁷⁻¹⁹ related with a high hydrogen surface coverage. On the other hand, it is worth mentioning that, beyond ethylene hydrogenation, the surface as-formed CH_3 -moiety at $\theta_{\text{H}} = 0.88$ ML could also form methane (CH_4) —see Figure S9 and its associated discussion in the SI—, yet displaying an energy barrier more than twice higher than the final C_2H_6 formation; therefore, one would expect to detect significant amounts of methane together with ethane, yet coming from the δ -MoC surface decarburization rather than as a direct product coming from ethylene.

To finally complete the catalytic cycle, the as-formed ethane must desorb from the surface. The ethane desorption rate was calculated at each coverage, see Figure S10 and Table S3 of the SI. The desorption rates are sufficiently large so that this step does not limit the overall process. Note that thermodynamic arguments, as observed in Figure 4, suggest that the working temperature should be below 400 K. Figure 6 shows that the ethane desorption rate is clearly linked to the adsorption strength, with the fastest desorption corresponding to $\theta_{\text{H}} = 0.13$ ML, where the interaction between ethane and that underlying carbide surface is the weakest. In the 300-400 K range, relevant for working temperature, the ethane desorption rate decreases with increasing θ_{H} , see Figure 6. Note that, even for the most unfavorable situation of $\theta_{\text{H}} = 0.88$ ML, the desorption rate is around $4 \cdot 10^{11} \text{ s}^{-1}$, much larger than the reaction rate of the limiting step of around 10^3 s^{-1} . Consequently, once ethane is formed, one expects to be readily desorbed, thus completing the catalytic cycle.

The present results illustrate the unique role that the hydrogen coverage can play on a carbide surface during the hydrogenation of an olefin. On δ -MoC(001), the relatively small energy barrier of 0.68 eV for H_2 dissociation^{Error! Marcador no definido.} opens the door for large H coverages (> 0.4 ML) leading to a very efficient system for ethylene hydrogenation. In the past, ethylene adsorption has been studied on some TMCs,²⁴ and its hydrogenation partially explored on TaC²⁵ and WC²⁶ based catalysts, but here we have provided the first detailed study for the C_2H_4 hydrogenation reaction mechanism over a carbide showing characteristics or features not seen on metal catalysts. These can be exploited when dealing with technical or industrial applications.

CONCLUSIONS

The hydrogenation mechanism of ethylene on a δ -MoC (001) surface catalyst at several hydrogen surface coverages has been investigated by means of periodic DFT calculations. *Ab initio* thermodynamics has been used to explore the effect of the ethylene partial pressure and temperature on ethylene adsorption, with elementary reaction and ethane desorption rates estimated from transition state theory within the harmonic approximation.

For the lowest hydrogen coverage considered, the ethylene hydrogenation reaction mechanism is complex involving several hydrogen migration and isomerization steps. In this situation, the second hydrogenation step; $C_2H_5^* + H^* \rightarrow C_2H_6^*$, involves a large energy barrier of 1.71 eV, due to the energetic toll paid to break a strong covalent bond between the ethyl intermediate and a surface C atom. Increasing the hydrogen coverage forces H^* to occupy all surface C and Mo atoms,¹³ and for the largest hydrogen coverage considered, 0.88 ML, the adsorbed H^* atoms reorganize leading to CH_3 type surface entities that contribute largely stabilizing the adsorbed C_2H_4 , actually favoring the subsequent hydrogenation of ethyl to adsorbed ethane.

The *ab initio* thermodynamics analysis has been employed to analyze whether adsorbed ethylene becomes stable at different hydrogen coverages on a set of relevant values of ethylene partial pressures and temperatures. The results indicate that for zero and high (0.88 ML) hydrogen coverage, ethylene adsorption is favored from very low to evaluated pressures (10^{-10} to 100 atm) in a broad range of temperatures (25 to 1200 K). However, for low and intermediate hydrogen coverages, 0.13 and 0.50 ML, respectively, ethylene adsorption at 300 K becomes non-favored in a broad range of pressures. However, for the hydrogen high coverage situation (0.88 ML) and 1 atm, ethylene adsorption becomes feasible only at temperatures below 400 K due to an interaction with the CH_3 surface entities.

The reaction mechanism was studied for the three representative H coverage situations. The results show that, for the first hydrogenation step, the energy barriers are rather insensitive to the hydrogen coverage; *i.e.* 0.59 eV for $\theta_H = 0.88$ ML compared to 0.47 and 0.40 eV for $\theta_H = 0.13$ and 0.50 ML, respectively. However, the energy barrier for the second hydrogenation exhibits an extremely large dependence on the hydrogen coverage dropping from 1.71 eV at $\theta_H = 0.13$ ML, to 0.36 eV at $\theta_H = 0.50$ ML to a very small value of 0.08 eV for $\theta_H = 0.88$ ML. It is worth noting that these values are also below the corresponding values predicted for Pt (111) —0.49 and 0.55 eV for first and second hydrogenation steps, respectively—^{49,51} and Pd (111) —0.55 and 0.52 eV—^{49,51} suggesting δ -MoC as a suitable replacement to scarce and expensive Pt- and Pd-based catalysts for olefin hydrogenation, provided high hydrogen surface coverage conditions are ensured. The present results pave the road to further address more complex systems, and could also

serve as a benchmark for future experimental studies, given the so far lack of experimental information for ethylene hydrogenation on δ -MoC (001).

ASSOCIATED CONTENT

Supporting Information

The following Supporting Information is available free of charge on the ACS Publications website at DOI:

Details on the surface models used to represent the evaluated hydrogen coverage situations, atomic structure of reactants, intermediates, and products for three coverage situations explored, full description of the hydrogenation mechanism as a function of hydrogen coverage including additional tables and figures. Additional information regarding the calculation of ethylene adsorption energy and thermodynamic properties, reaction rates, and ethane desorption rates.

ACKNOWLEDGMENTS

The research carried out at the *Universitat de Barcelona* has been supported by the Spanish MICIUN/FEDER RTI2018-095460-B-I00 and María de Maeztu MDM-2017-0767 grants and, in part, by *Generalitat de Catalunya* 2017SGR13 and XRQTC grants. C. J.-O. and E. F. acknowledge to Universidad de Medellín for financial support, F. V. is thankful to *Ministerio de Economía y Competitividad* (MINECO) for his *Ramón y Cajal* (RYC-2012-10129) research contract, and F. I. acknowledges additional support from the 2015 ICREA Academia Award for Excellence in University Research. Part of this research used resources of the Center for Functional Nanomaterials, which is a U.S. DOE Office of Science Facility, and the Scientific Data and Computing Center, a component of the Computational Science Initiative, at Brookhaven National Laboratory under Contract No. DE-SC0012704. Computational resources provided by the *Consorti de Serveis Universitaris de Catalunya* (CSUC) are fully acknowledged.

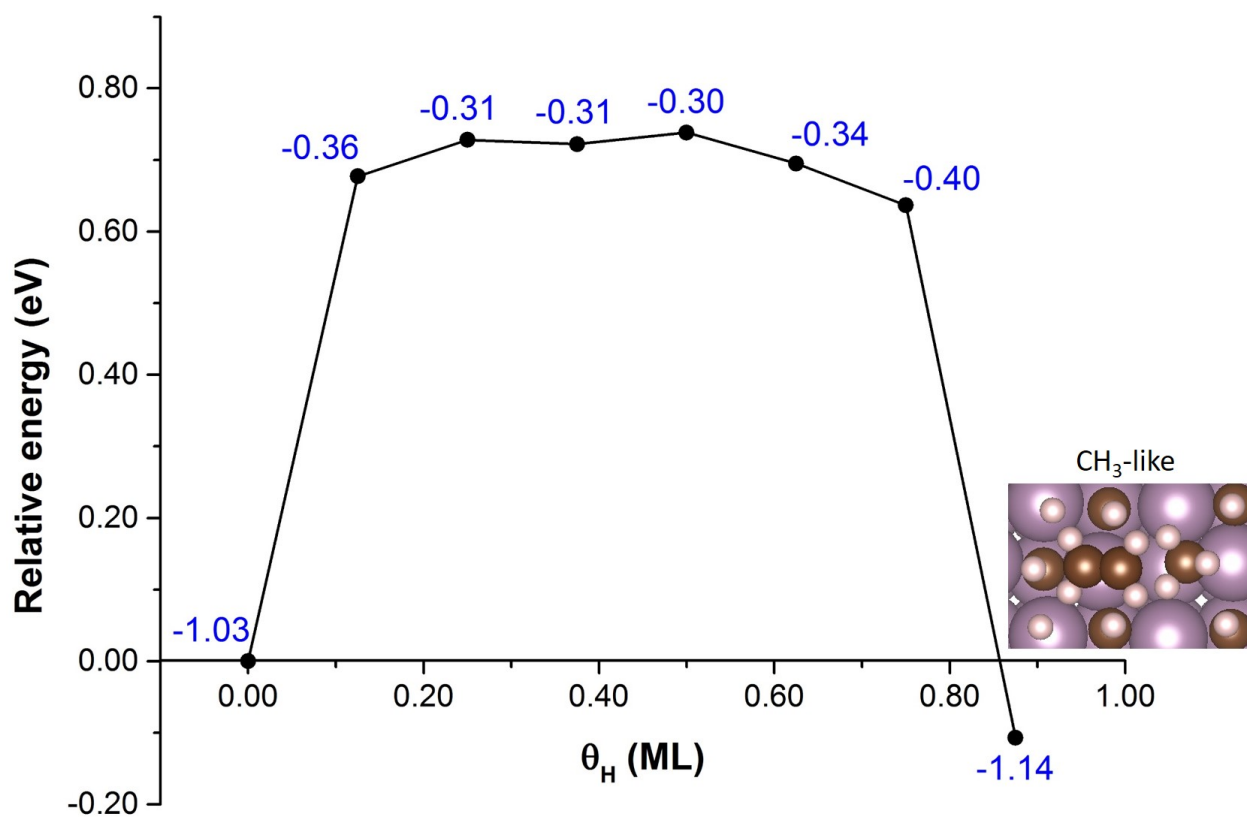


Figure 1. Dependence of the C_2H_4 binding energy on the θ_H coverage relative to that on the clean δ -MoC (001) surface of -1.03 eV. The respective ethylene adsorption energy (in eV) is shown in blue near the points. A top view of the ethylene binding geometry at $\theta_H = 0.88$ ML is included. Mo, C, and H atoms are represented as magenta, brown, and light gray color spheres, respectively.

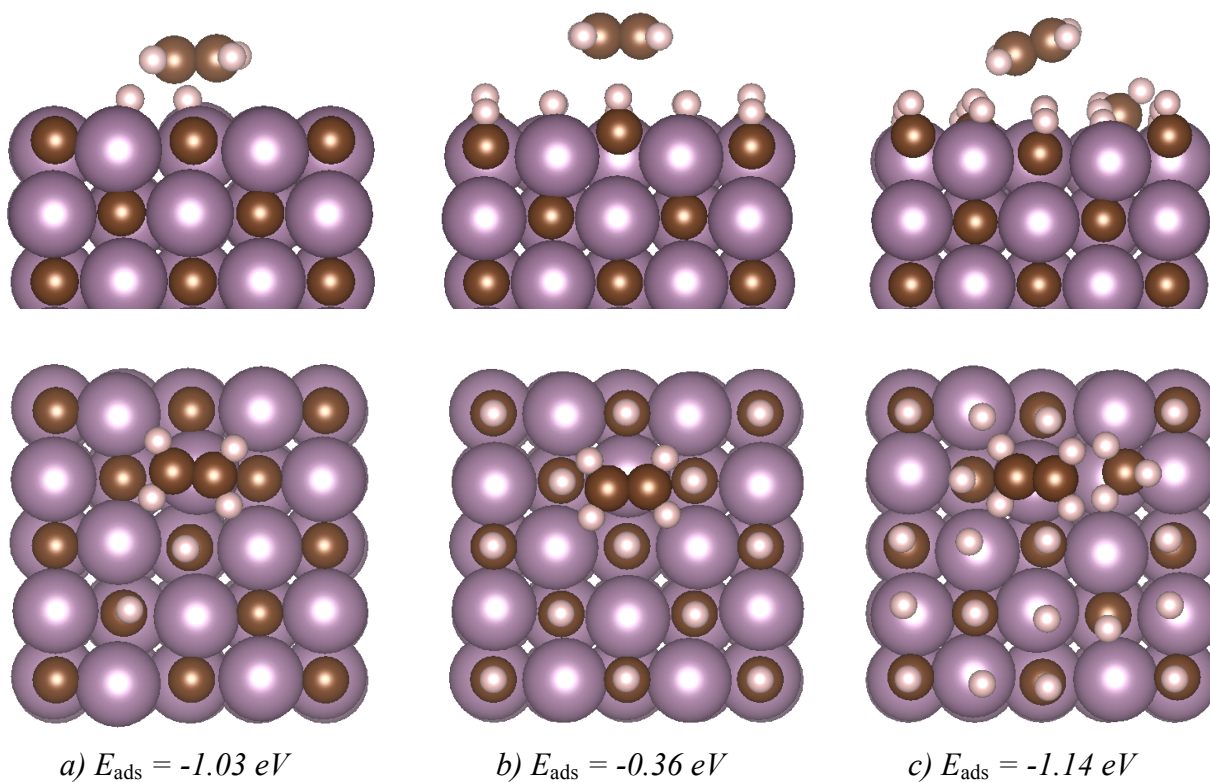


Figure 2. Ethylene adsorption energy on $\delta\text{-MoC}(001)$, E_{ads} , at three θ_{H} coverage states; *a)* 0.13, *b)* 0.50, and *c)* 0.88 ML. Side (top) and top (bottom) views are shown. Color coding as in Figure 1.

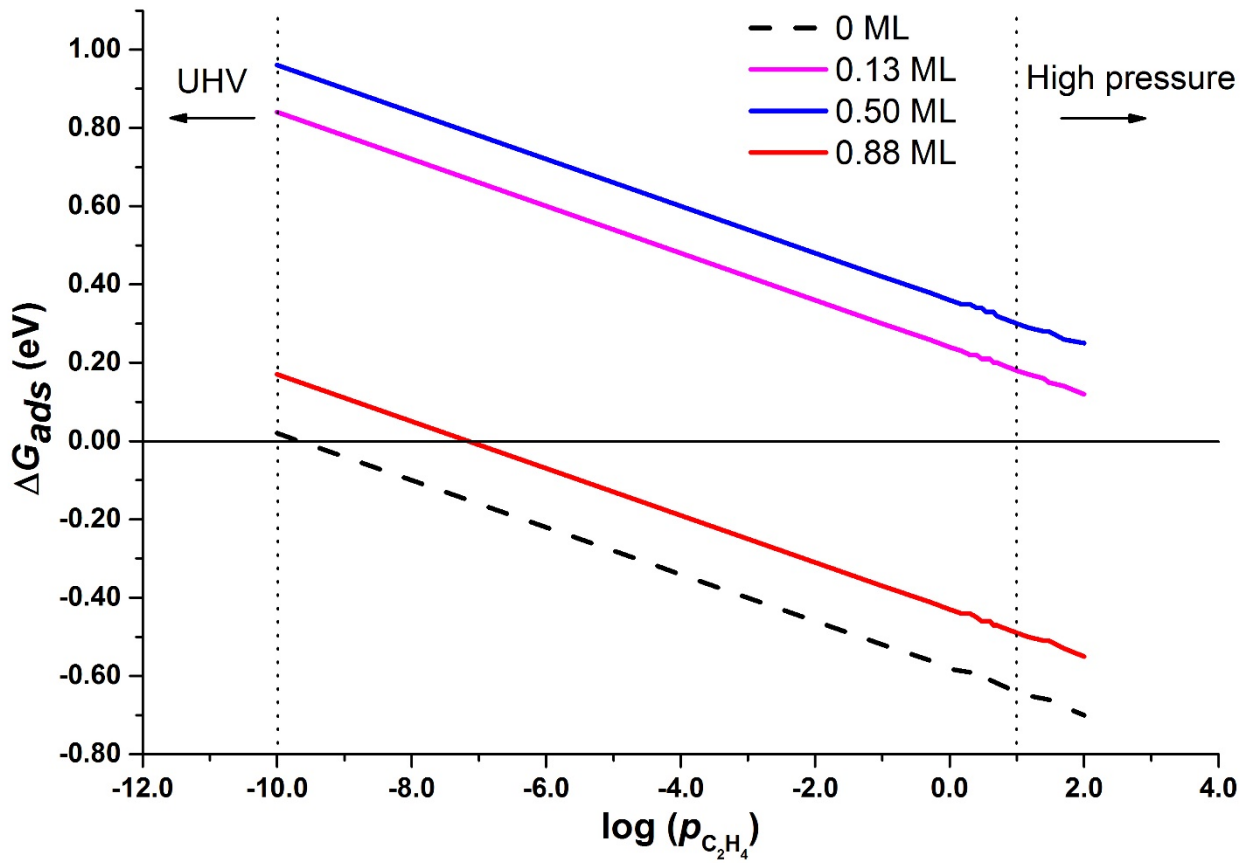


Figure 3. Effect of $p_{C_2H_4}$ on the C_2H_4 adsorption Gibbs free energy on δ -MoC(001), ΔG_{ads} , at 300 K and for different θ_H coverage. The vertical dotted lines indicate the limits of low (ultrahigh vacuum) and high pressures, respectively.

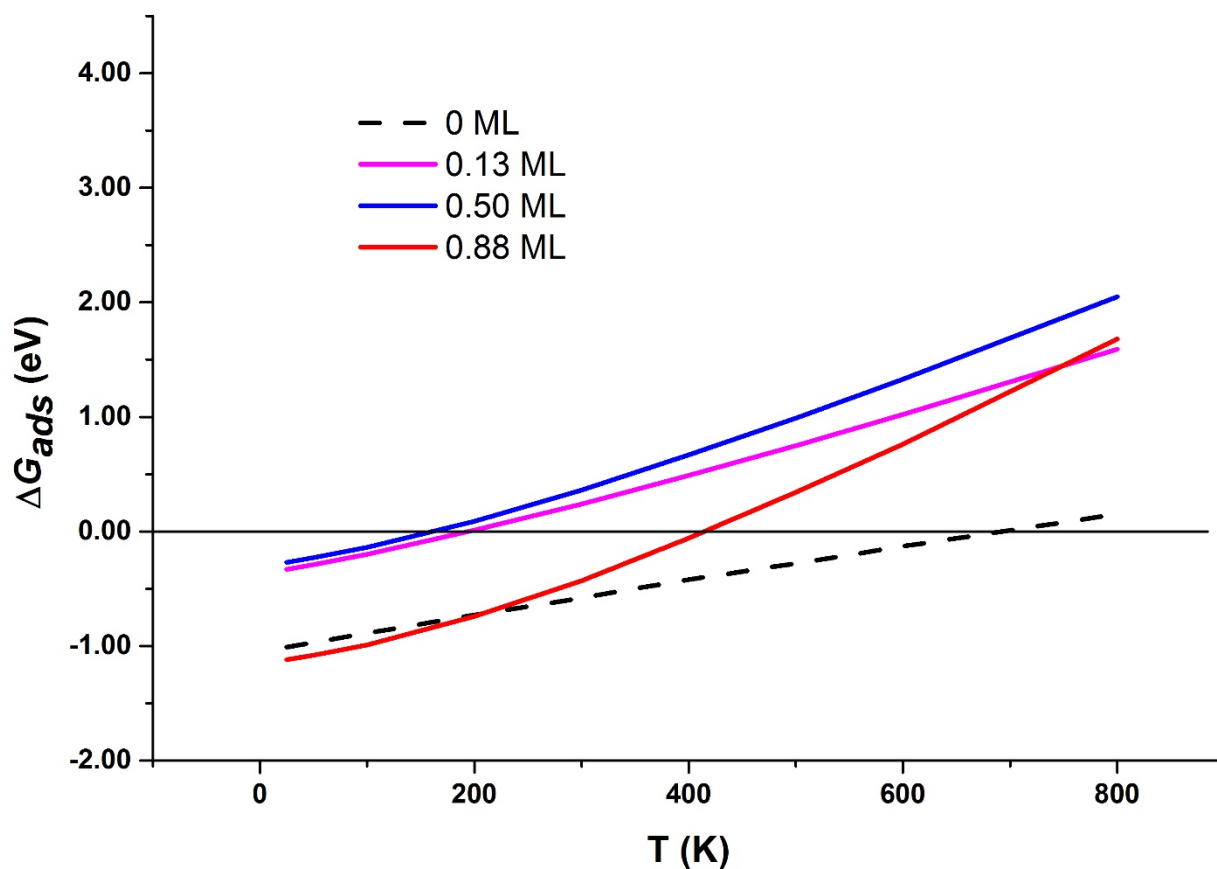


Figure 4. Temperature effect in the C_2H_4 adsorption Gibbs free energy on δ -MoC(001), ΔG_{ads} , at 1 atm of $p_{C_2H_4}$ and for different θ_H coverages.

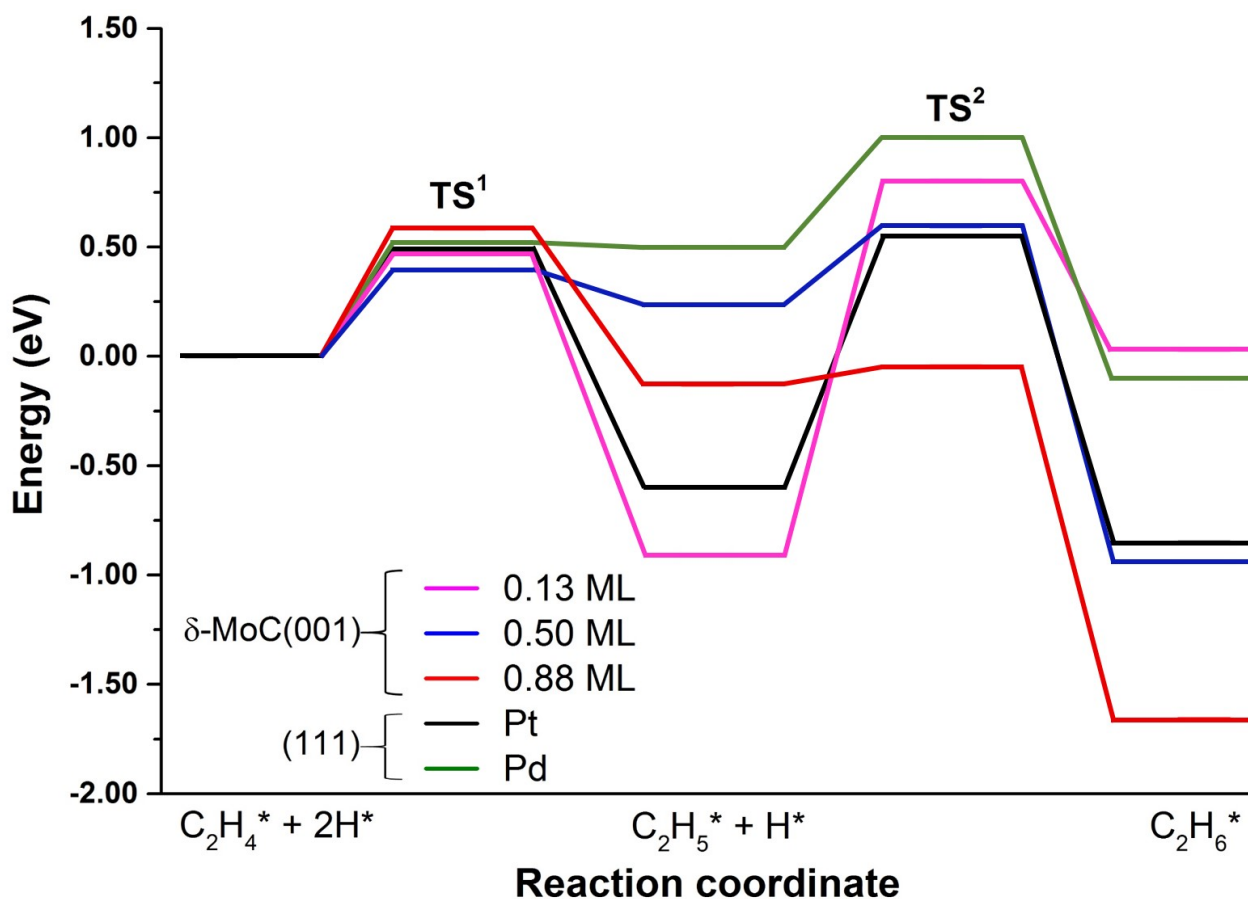


Figure 5. Reaction energy profile for the two hydrogenation steps of C_2H_4 when adsorbed on δ -MoC (001) at θ_H of 0.13, 0.50, and 0.88 ML. Values for Pt and Pd (111) surfaces are taken from the literature and included for comparison.¹ For convenience, H^* migration and intermediate isomerization steps are not reported, yet these are clearly represented in Figure S4 of the SI.

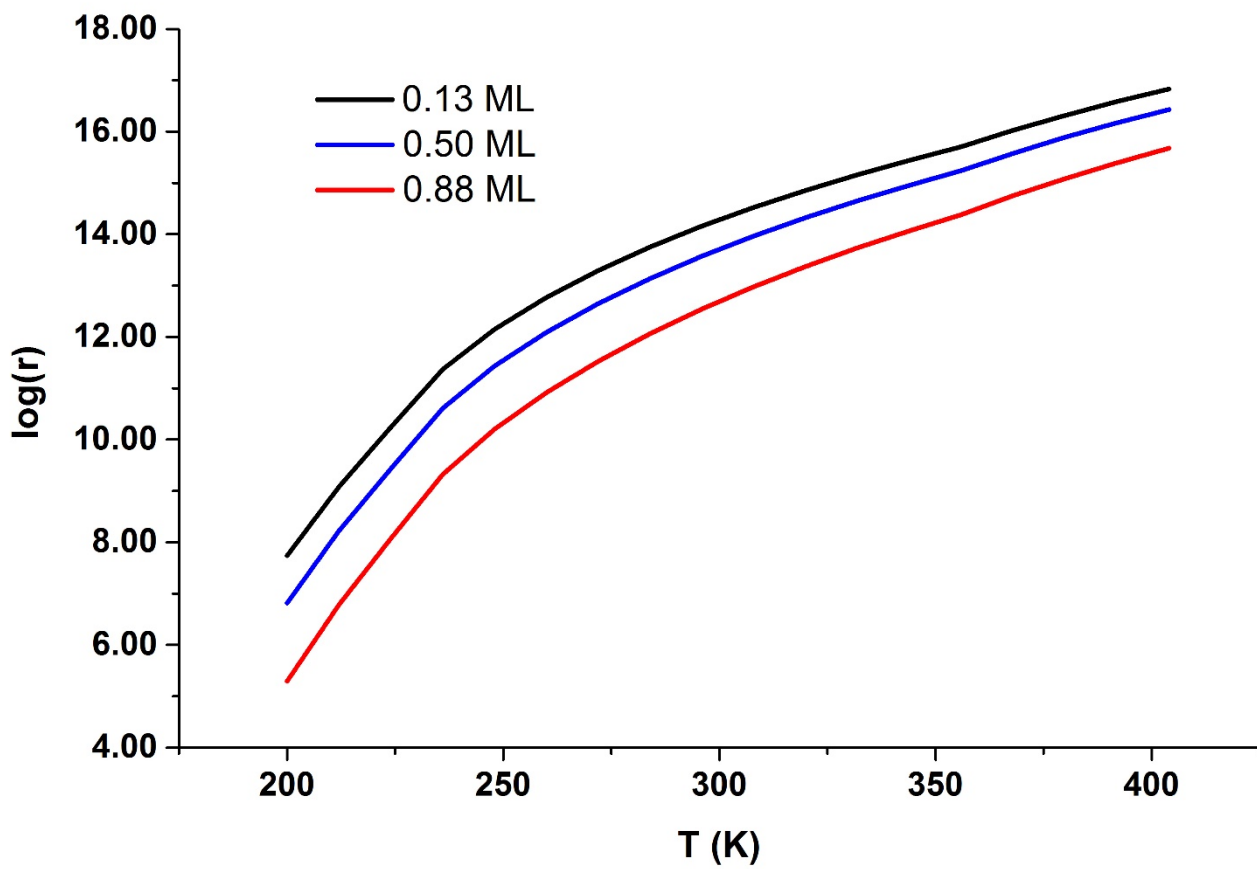


Figure 6. Logarithm of the ethane desorption rate, in s^{-1} , as a function of θ_H for temperatures in range 200–400 K.

References

- (1) Wilson, J. N.; Otvos, J. W.; Stevenson, D. P.; Wagner, C. D. Hydrogenation of Olefins over Metals. *Ind. Eng. Chem.* **1953**, *45*, 1480–1487.
- (2) Dhandapani, B.; St. Clair, T.; Oyama, S. T. Simultaneous Hydrodesulfurization, Hydrodeoxygenation, and Hydrogenation with Molybdenum Carbide. *Appl. Catal. A Gen.* **1998**, *168*, 219–228.
- (3) Hwu, H. H.; Chen, J. G. Surface Chemistry of Transition Metal Carbides. *Chem. Rev.* **2005**, *105*, 185–212.
- (4) Levy, R. .; Boudart, M. Platinum-Like Behavior of Tungsten Carbide in Surface Catalysis. *Science* **1973**, *181*, 547–549.
- (5) Oyama, S. T. *The Chemistry of Transition Metal Carbide and Nitrides*, 1st ed.; Blackie academic & professional, Wester Cleddens Road, Bishopbriggs, Glasgow G64 2NZ, UK, **1996**, 1.
- (6) Posada-Pérez, S.; Viñes, F.; Ramirez, P. J.; Vidal, A. B.; Rodriguez, J. A.; Illas, F. The Bending Machine: CO₂ Activation and Hydrogenation on δ -MoC(001) and β -Mo₂C(001) Surfaces. *Phys. Chem. Chem. Phys.* **2014**, *16*, 14912-14921.
- (7) Frauwallner, M. L.; López-Linares, F.; Lara-Romero, J.; Scott, C. E.; Ali, V.; Hernández, E.; Pereira-Almao, P. Toluene Hydrogenation at Low Temperature Using a Molybdenum Carbide Catalyst. *Appl. Catal. A Gen.* **2011**, *394*, 62–70.
- (8) Ardakani, S. J.; Liu, X.; Smith, K. J. Hydrogenation and Ring Opening of Naphthalene on Bulk and Supported Mo₂C Catalysts. *Appl. Catal. A Gen.* **2007**, *324*, 9–19.
- (9) Lin, L.; Zhou, W.; Gao, R.; Yao, S.; Zhang, X.; Xu, W.; Zheng, S.; Jiang, Z.; Yu, Q.; Li, Y.-W.; Shi, C.; Wen, X. D.; Ma, D. Low-Temperature Hydrogen Production from Water and Methanol Using Pt/ α -MoC Catalysts. *Nature* **2017**, *544*, 80–83.
- (10) Rodriguez, J. A.; Ramírez, P. J.; Gutierrez, R. A. Highly Active Pt/MoC and Pt/TiC Catalysts for the Low-Temperature Water-Gas Shift Reaction: Effects of the Carbide Metal/Carbon Ratio on the Catalyst Performance. *Catal. Today* **2017**, *289*, 47–52.
- (11) Posada-Pérez, S.; Ramírez, P. J.; Evans, J.; Viñes, F.; Liu, P.; Illas, F.; Rodriguez, J. A. Highly Active Au/ δ -MoC and Cu/ δ -MoC Catalysts for the Conversion of CO₂: The Metal/C Ratio as a Key Factor Defining Activity, Selectivity, and Stability. *J. Am. Chem. Soc.* **2016**, *138*, 8269–8278.
- (12) Yao, S.; Zhang, X.; Zhou, W.; Gao, R.; Xu, W.; Ye, Y.; Lin, L.; Wen, X.; Liu, P.; Chen, B.; Crumlin, E.; Guo, J.; Zuo, Z.; Li, W.; Xie, J.; Lu, L.; Kiely, C.J.; Gu, L.; Shi, C.; Rodriguez, J. A.; Ma, D. Atomic-Layered Au Clusters on α -MoC as Catalysts for the Low-Temperature Water-Gas Shift Reaction. *Science* **2017**, *357*, 389–393.

- (13) Posada-Pérez, S.; Viñes, F.; Valero, R.; Rodriguez, J. A.; Illas, F. Adsorption and Dissociation of Molecular Hydrogen on Orthorhombic β -Mo₂C and Cubic δ -MoC (001) Surfaces. *Surf. Sci.* **2017**, *656*, 24–32.
- (14) Prats, H.; Piñero, J. J.; Viñes, F.; Bromley, S. T.; Sayós, R.; Illas, F. Assessing the Usefulness of Transition Metal Carbides for Hydrogenation Reactions. *Chem. Commun.* **2019**, *55*, 12797–12800.
- (15) Viñes, F.; Sousa, C.; Liu, P.; Rodriguez, J. A.; Illas, F. A Systematic Density Functional Theory Study of the Electronic Structure of Bulk and (001) Surface of Transition-Metals Carbides. *J. Chem. Phys.* **2005**, *122*, 174709.
- (16) Quesne, M. G.; Roldan, A.; de Leeuw, N. H.; Catlow, C. R. A. Bulk and Surface Properties of Metal Carbides: Implications for Catalysis. *Phys. Chem. Chem. Phys.* **2018**, *20*, 6905–6916.
- (17) Cremer, P. S.; Su, X. C.; Shen, Y. R.; Somorjai, G. a. Ethylene Hydrogenation on Pt(111) Monitored in Situ at High Pressures Using Sum Frequency Generation. *J. Am. Chem. Soc.* **1996**, *118*, 2942–2949.
- (18) Rekoske, J. E.; Cortright, R. D.; Goddard, S. A.; Sharma, S. B.; Dumesic, J. A. Microkinetic Analysis of Diverse Experimental Data for Ethylene Hydrogenation on Platinum. *J. Phys. Chem.* **1992**, *96*, 1880–1888.
- (19) Cortright, R. D.; Goddard, S. A.; Rekoske, J. E.; Dumesic, J. A. Kinetic Study of Ethylene Hydrogenation. *J. Catal.* **1991**, *127*, 342–353.
- (20) Godbey, D.; Zaera, F.; Yeates, R.; Somorjai, G. A. Hydrogenation of Chemisorbed Ethylene on Clean, Hydrogen, and Ethylidyne Covered Platinum (111) Crystal Surfaces. *Surf. Sci.* **1986**, *167*, 150–166.
- (21) Mei, D.; Sheth, P. A.; Neurock, M.; Smith, C. M. First-Principles-Based Kinetic Monte Carlo Simulation of the Selective Hydrogenation of Acetylene over Pd(111). *J. Catal.* **2006**, *242*, 1–15.
- (22) Molero, H.; Stacchiola, D.; Tysoe, W. T. The Kinetics of Ethylene Hydrogenation Catalyzed by Metallic Palladium. *Catal. Letters* **2005**, *101*, 145–149.
- (23) Stacchiola, D.; Tysoe, W. T. The Effect of Subsurface Hydrogen on the Adsorption of Ethylene on Pd(1 1 1). *Surf. Sci.* **2003**, *540*, L600–L604.
- (24) Jimenez-Orozco, C.; Flórez, E.; Montoya, A.; Rodriguez, J. A. Binding and Activation of Ethylene on Tungsten Carbide and Platinum Surfaces. *Phys. Chem. Chem. Phys.* **2019**, *21*, 17332–17342.
- (25) Kojima, I.; Miyakasi, E.; Yasunobu, I.; Yasumori, I. Catalysis by Transition Metal Carbides: IV. Mechanism of Ethylene Hydrogenation and the Nature of Active Sites on Tantalum Monocarbide. *J. Catal.* **1982**, *73*, 128–135.

- (26) Cui, X.; Zhou, X.; Chen, H.; Hua, Z.; Wu, H.; He, Q.; Zhang, L.; Shi, J. In-Situ Carbonization Synthesis and Ethylene Hydrogenation Activity of Ordered Mesoporous Tungsten Carbide. *Int. J. Hydrogen Energy* **2011**, *36*, 10513–10521.
- (27) Jimenez-Orozco, C.; Florez, E.; Moreno, A.; Liu, P.; Rodriguez, J. A. Systematic Theoretical Study of Ethylene Adsorption on δ -MoC(001), TiC(001), and ZrC(001) Surfaces. *J. Phys. Chem. C* **2016**, *120*, 13531–13540.
- (28) Zaera, F.; Somorjai, G. A. Hydrogenation of Ethylene over Platinum (111) Single-Crystal Surfaces. *J. Am. Chem. Soc.* **1984**, *106*, 2288–2293.
- (29) Jimenez-Orozco, C.; Florez, E.; Moreno, A.; Rodriguez, J. A. Platinum vs Transition Metal Carbide Surfaces as Catalysts for Olefin and Alkyne Conversion: Binding and Hydrogenation of Ethylidyne. *J. Phys. Conf. Ser.* **2019**, *1247*, 012003.
- (30) Zaera, F. Key Unanswered Questions about the Mechanism of Olefin Hydrogenation Catalysis by Transition-Metal Surfaces: A Surface-Science Perspective. *Phys. Chem. Chem. Phys.* **2013**, *15*, 11988–12003.
- (31) Piñero, J. J.; Ramírez, P. J.; Bromley, S. T.; Illas, F.; Viñes, F.; Rodriguez, J. A. Diversity of Adsorbed Hydrogen on the TiC(001) Surface at High Coverages. *J. Phys. Chem. C* **2018**, *122*, 28013–28020.
- (32) Reuter, K.; Scheffler, M. Composition, Structure, and Stability of RuO₂(110) as a Function of Oxygen Pressure. *Phys. Rev. B* **2001**, *65*, 035406.
- (33) Reuter, K.; Scheffler, M. Composition and Structure of the RuO₂(110) Surface in an O₂ and CO Environment: Implications for the Catalytic Formation of CO₂. *Phys. Rev. B* **2003**, *68*, 045407.
- (34) Kunkel, C.; Viñes, F.; Illas, F. Transition Metal Carbides as Novel Materials for CO₂ Capture, Storage, and Activation. *Energy Environ. Sci.* **2016**, *9*, 141–144.
- (35) Rodriguez, J. A.; Liu, P.; Gomes, J.; Nakamura, K.; Viñes, F.; Sousa, C.; Illas, F. Interaction of Oxygen with ZrC(001) and VC(001): Photoemission and First-Principles Studies. *Phys. Rev. B* **2005**, *72*, 075427.
- (36) Viñes, F.; Rodriguez, J. A.; Liu, P.; Illas, F. Catalyst Size Matters: Tuning the Molecular Mechanism of the Water–Gas Shift Reaction on Titanium Carbide Based Compounds. *J. Catal.* **2008**, *260*, 103–112.
- (37) Kresse, G.; Furthmüller, J. Efficient Iterative Schemes for Ab Initio Total-Energy Calculations Using a Plane-Wave Basis Set. *Phys. Rev. B* **1996**, *54*, 11169–11186.
- (38) Perdew, J. P.; Burke, K.; Ernzerhof, M. Generalized Gradient Approximation Made Simple. *Phys. Rev. Lett.* **1996**, *77*, 3865–3868.
- (39) Politi, J. R. D. S.; Viñes, F.; Rodriguez, J. A.; Illas, F. Atomic and Electronic Structure of

- Molybdenum Carbide Phases: Bulk and Low Miller-Index Surfaces. *Phys. Chem. Chem. Phys.* **2013**, *15*, 12617.
- (40) Grimme, S.; Antony, J.; Ehrlich, S.; Krieg, H. A Consistent and Accurate Ab Initio Parametrization of Density Functional Dispersion Correction (DFT-D) for the 94 Elements H-Pu. *J. Chem. Phys.* **2010**, *132*, 154104.
- (41) Blöchl, P. E. Projector Augmented-Wave Method. *Phys. Rev. B* **1994**, *50*, 17953–17979.
- (42) Kresse, G.; Joubert, D. From Ultrasoft Pseudopotentials to the Projector Augmented-Wave Method. *Phys. Rev. B* **1999**, *59*, 1758–1775.
- (43) Monkhorst, H. J.; Pack, J. D. Special Points for Brillouin-Zone Integrations. *Phys. Rev. B* **1976**, *13* (12), 5188–5192.
- (44) Hjorth Larsen, A.; Jørgen Mortensen, J.; Blomqvist, J.; Castelli, I. E.; Christensen, R.; Dułak, M.; Friis, J.; Groves, M. N.; Hammer, B.; Hargus, C.; et al. The Atomic Simulation Environment—a Python Library for Working with Atoms. *J. Phys. Condens. Matter* **2017**, *29*, 273002.
- (45) Henkelman, G.; Uberuaga, B. P.; Jónsson, H. A Climbing Image Nudged Elastic Band Method for Finding Saddle Points and Minimum Energy Paths. *J. Chem. Phys.* **2000**, *113*, 9901–9904.
- (46) Chorkendorff, I.; Niemantsverdriet, J. Concepts of Modern Catalysis and Kinetics; WILEY-VCH Verlag GmbH & Co. KGaA: Weinheim, **2003**.
- (47) Nørskov, J. K.; Studt, F.; Abild-Pedersen, F.; Bligaard, T. Fundamental Concepts in Heterogeneous Catalysis; John Wiley & Sons, Inc., **2014**.
- (48) Plata, J. J.; Collico, V.; Márquez, A. M.; Sanz, J. F. Analysis of the Origin of Lateral Interactions in the Adsorption of Small Organic Molecules on Oxide Surfaces. *Theor. Chem. Acc.* **2013**, *132*, 1311.
- (49) Heard, C. J.; Siahrostami, S.; Grönbeck, H. Structural and Energetic Trends of Ethylene Hydrogenation over Transition Metal Surfaces. *J. Phys. Chem. C* **2016**, *120*, 995–1003.
- (50) Heard, C. J.; Hu, C.; Skoglundh, M.; Creaser, D.; Grönbeck, H. Kinetic Regimes in Ethylene Hydrogenation over Transition-Metal Surfaces. *ACS Catal.* **2016**, *6*, 3277–3286.
- (51) Jørgensen, M.; Grönbeck, H. Selective Acetylene Hydrogenation over Single-Atom Alloy Nanoparticles by Kinetic Monte Carlo. *J. Am. Chem. Soc.* **2019**, *141*, 8541–8549.
- (52) Shi, Q.; Sun, R. Adsorption Manners of Hydrogen on Pt(100), (110) and (111) Surfaces at High Coverage. *Comput. Theor. Chem.* **2017**, *1106*, 43–49.
- (53) Vasić, D.; Ristanović, Z.; Pašti, I.; Mentus, S. Systematic DFT-GGA Study of Hydrogen Adsorption on Transition Metals. *Russ. J. Phys. Chem. A* **2011**, *85*, 2373–2379.
- (54) Sabbe, M. K.; Canduela-Rodriguez, G.; Reyniers, M.-F.; Marin, G. B. DFT-Based Modeling

of Benzene Hydrogenation on Pt at Industrially Relevant Coverage. *J. Catal.* **2015**, *330*, 406–422.

- (55) Meemken, F.; Baiker, A.; Dupré, J.; Hungerbühler, K. Asymmetric Catalysis on Cinchonidine-Modified Pt/Al₂O₃: Kinetics and Isotope Effect in the Hydrogenation of Trifluoroacetophenone. *ACS Catal.* **2014**, *4*, 344–354.

Table of Contents

